Society For Biomaterials

A computational model for stress reduction at the skin-implant interface of osseointegrated prostheses

Srinivasu Yerneni,[1,2] Yasin Dhaher,[2,3] Todd A. Kuiken[1,2,3]

[1]Center for Bionic Medicine, Rehabilitation Institute of Chicago, Chicago, Illinois 60611
[2]Department of Biomedical Engineering, Northwestern University, Evanston, Illinois 60208
[3]Department of Physical Medicine and Rehabilitation, Northwestern University, Chicago, Illinois 60611

Received 3 January 2011; revised 13 June 2011; accepted 11 November 2011
Published online 24 January 2012 in Wiley Online Library (wileyonlinelibrary.com). DOI: 10.1002/jbm.a.34028

Abstract: Osseointegrated implants (OI)s for transfemoral prosthetic attachment offer amputees an alternative to the traditional socket attachment. Potential benefits include a natural transfer of loads directly to the skeleton via the percutaneous abutment, relief of pain and discomfort of residual limb soft tissues by eliminating sockets, increased sensory feedback, and improved function. Despite the benefits, the skin-implant interface remains a critical limitation, as it is highly prone to bacterial infection. One approach to improve clinical outcomes is to minimize stress concentrations at the skin-implant interface due to shear loading, reducing soft tissue breakdown and subsequent risk of infection. We hypothesized that broadening the bone base at the distal end of the femur would provide added surface area for skin adhesion and reduce stresses at the skin-implant interface. We tested this hypothesis using finite element models of an OI in a residual limb. Results showed a dramatic decrease in stress reduction, with up to ~90% decrease in stresses at the skin-implant interface as cortical bone thickness increased from 2 to 8 mm. The findings in this study suggests that surgical techniques could stabilize the skin-implant interface, thus enhancing a skin-to-bone seal around the percutaneous device and minimizing infection. J Biomed Mater Res Part A: 100A: 911–917, 2012.

Key Words: osseointegration, prostheses, finite, skin-implant, stresses

How to cite this article: Yerneni S, Dhaher Y, Kuiken TA. 2012. A computational model for stress reduction at the skin-implant interface of osseointegrated prostheses. J Biomed Mater Res Part A 2012:100A:911–917.

INTRODUCTION

Osseointegrated implants (OI)s provide an alternative method for prosthetic attachment that alleviates many of the problems associated with the traditional socket. For a transfemoral amputee, OIs are inserted directly into the medullary canal of the residual bone. With time, they become integrated so that there is no relative movement between the implant and femur.[1–7] A metal rod, called an abutment, is then attached to the implant, protrudes through the skin and provides attachment for the prosthesis. Thus, loads due to ambulation are transferred directly from the prosthesis to the skeleton, relieving stress, and pain in the soft tissues of the limb. In addition, the intimate connection to the skeleton enhances hip proprioception and increases sensory feedback. This feedback, called "osseoperception," improves the functionality of the prosthesis.[5]

Although osseointegration has many advantages over socket usage, there are a number of potential disadvantages with this approach. Primarily, the exit site through the skin leaves a permanent opening for bacterial infection that can necessitate removal of the implant.[2,4,8,9] Thus, maintaining a clean environment at the skin-implant interface is crucial for the success and longevity of the implant. Much of the current research addressing infection has focused on creating a seal between the skin and the implant by promoting epithelial cell growth into the implant, thereby closing off the exit site to bacterial infection. Preliminary studies show promising results, yet none are conclusive.[2,4,9–11]

Another area of concern that has been given little attention is the concentration of stresses at the skin-implant interface due to shear loading, which can increase risk of infection due to soft tissue breakdown. Stabilizing the skin is an attractive concept for buffering the stress at the skin-abutment interface. This could potentially be achieved by having the skin scar down to the surrounding cortical bone or by having the skin grow into a biocompatible material, such as porous titanium.[12] How large of an area that would be needed to adequately stabilize the skin is an unknown factor. Although skin can readily adhere to bone tissue, typically only 2–3 mm of cortical bone remain after implant insertion. We hypothesized that increasing bone surface area circumferentially around the distal portion of the femur would reduce stress concentrations at the skin-implant interface. The increased cortical bone thickness would serve as a mechanical stabilizer by dissipating stresses away from the skin-implant interface and help maintain the integrity of

Correspondence to: T. A. Kuiken; e-mail: tkuiken@northwestern.edu
Contract grant sponsors: McCormick Tribune Foundation and Rice Foundation

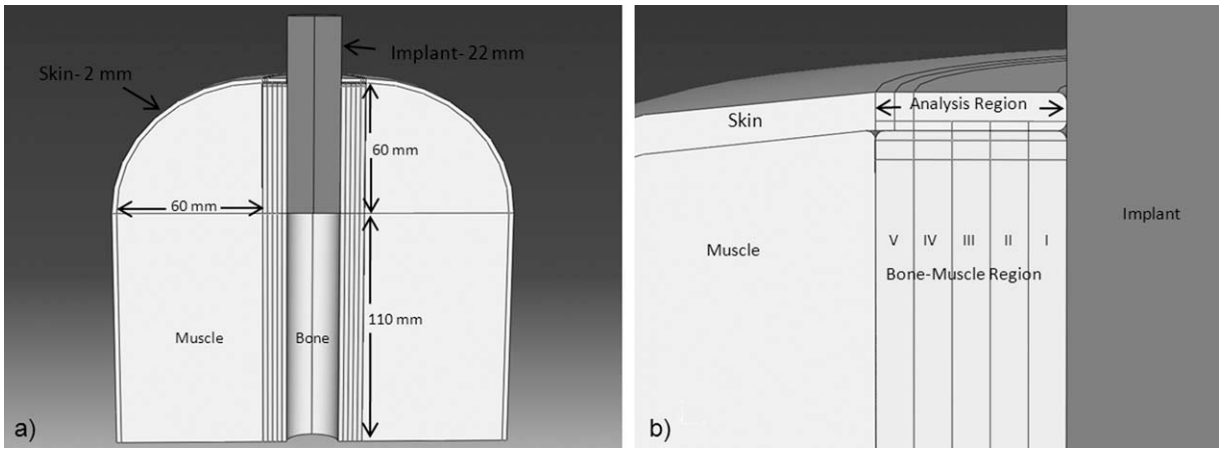

FIGURE 1. CAD model. (a) Hemisection of model. (b) Analysis region at skin–bone interface.

skin adhesion near the exit site. Also, having a broader area for skin–bone adhesion would allow a tight seal between the skin and bone, preventing both lymphatic drainage and bacterial migration proximally.

The objective of this study was to examine the effects of shear loading at the skin-abutment interface. For this initial study, the finite element (FE) method was used to build simplified versions of an OI model of a transfemoral residual leg. We then varied the thickness of cortical bone surrounding the abutment and quantified stress reduction at the skin-abutment interface.

METHODS

CAD modeling

A three-dimensional CAD model of an idealized residual limb of an OI in a transfemoral amputee was created using FE software (ABAQUS/CAE 6.7-1 Dassault Systems, Lowell, MA). The model consisted of the diaphysis region of the femur, titanium implant, surrounding muscle, and skin layers. The subcutaneous fat layer was excluded in the model; this is consistent with surgical practices that remove fat before attaching the skin to the bone.[13] Boolean operations were performed to assemble the parts into a full model [Fig. 1(a)]. The femur was sectioned into five symmetrical concentric slices of 2-mm thickness in order to vary the amount of cortical bone at the distal end of the femur. To study the effects of added bone, each slice was sequentially assigned bone material properties, while the remaining slices were assigned muscle properties. For instance, for the 4-mm bone case, regions I and II in the bone–muscle region were assigned bone material properties, while regions III, IV, and V were assigned muscle properties [Fig. 1(b)]. Region V was always assigned muscle properties, since the 10-mm bone case was not studied. The skin layer had a uniform thickness of 2 mm throughout the model. The implant had a uniform diameter of 22 mm, with an inserted length of 60 mm, and abutment length of 30 mm.[14] The analysis region was defined as the 10-mm ring of skin wrapping around the implant and tied to the underlying bone and muscle layers [Fig. 1(b)]. The edges between adjacent parts were rounded by 0.5 mm [Fig. 1(b)] to avoid the effects of distorted stress values at sharp edges due to geometric singularities. Theoretical stresses at singularities approach infinity and can increase convergence time for a simulation.

Material properties

The titanium implant was modeled as a homogeneous linear elastic material with an elastic modulus of 115 GPa, and Poisson's ratio of 0.3.[3] The femur was assumed to be isotropic in the diaphysis region and was specified an elastic modulus of 18 GPa and Poisson's ratio of 0.3.[3] Based on a previous study, a hyperelastic Mooney–Rivlin model was used for the muscle layers, with coefficients of $C_{10} = 30$ kPa, $C_{01} = 10$ kPa, and bulk modulus of $K = 60$ kPa.[15] Skin typically behaves viscoelastically; however, since this study focused on quasistatic loading, the time-dependent characteristics of skin were neglected and a simplified Neo–Hookean model for the dermis was used, with parameters $C_{10} = 1.11$ MPa and $K = 29.6$ MPa.[16]

Loads, constraints, and boundary conditions

All parts were assumed to have no relative motion with one another and were constrained using the ABAQUS tie constraint. This assumption is consistent with osseointegration studies that show that the bone and implant become fully integrated after a 6-month rehabilitation period.[3,5,7,17] Although the skin and muscle exhibit a certain degree of slip during shear loading, this interaction was not investigated in this initial study and thus these parts were also tied. The 10-mm area of skin in the analysis region was also tied to the underlying bone based on surgical practices by clinicians.[13] In addition, the leading edge of the skin was left unbounded to the abutment; this assumption was guided by current surgical practices.[1,13] The proximal end of the bone was assumed to be fixed in all directions.

FE mesh

The FE mesh was created using linear tetrahedral elements. The analysis region was sliced 0.5 mm from the bone and meshed with 0.5 mm elements; a 0.5-mm slice of underlying

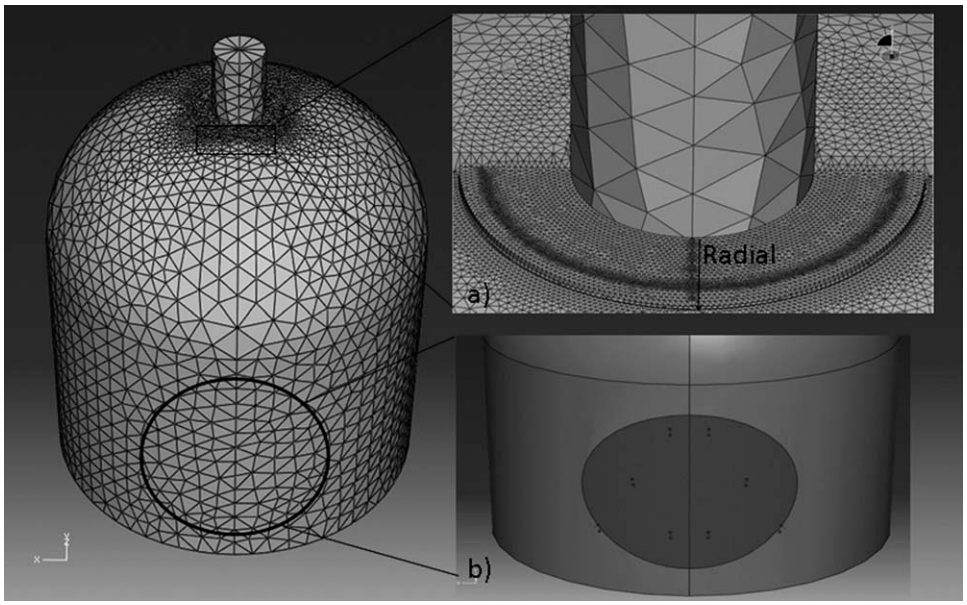

FIGURE 2. FE mesh. (a) Mesh refinement in region of interest along radial and circumferential directions for 8-mm bone case. The refinement areas are located at height (skin thickness) of 0.5 mm from the skin–bone interface. (b) Circular loading area for applied loads.

bone was also meshed with 0.5 mm elements to ensure mesh compatibility. Stress concentrations in the radial direction from the implant were of interest, thus this area was further refined with 0.2 mm elements based on a mesh convergence study, which examined the relative effects of element sizes ranging from 0.5 to 0.2 mm [Fig. 2(a)]. In addition, initial simulations indicated that stresses were concentrated within a 180° section of the analysis region at the bone–muscle boundary for each bone case. Thus, this area was also refined in the circumferential direction with 0.2 mm elements to ensure accurate analysis [Fig. 2(a)]. The remaining portion of the analysis region was specified with 1 mm elements. The remainder of the model consisted of elements ranging in size from 2 to 8 mm. The coarser elements in these areas greatly reduced simulation times without reducing accuracy of results in the analysis region. A total of ~225,000 elements were specified and the ABAQUS full Newtonian direct solver algorithm was used for the simulations.

To simulate physiological loading conditions, we proposed a hypothetical situation where a 75-kg person were sliding down a chair, with half body weight experienced at each leg in the midthigh region, at an angle of 45° from the horizontal. Under these conditions, the compressive and shear forces are equal and were calculated to be ~260 N at each leg. Using a circular loading area, 8 cm in diameter [Fig. 2(b)], the shear and compressive applied loads were calculated to be 51.8 kPa. This was considered maximum loading based on body weight. The loads were ramped linearly during the course of the simulation (Fig. 3). Loads that were 0.1 and 0.01 of maximum loading were also specified to study the effects of load variation on stress. Four bone cases of 2, 4, 6, and 8 mm were studied, yielding a total of 12 simulations.

RESULTS

Data were recorded as von Mises stresses along the radial direction in the analysis region [Fig. 2(a)], which was aligned symmetrically with the centerline of the circular loading zone [Fig. 2(b)]. The mesh convergence study, using the 2-mm bone case, showed a nonlinear relationship between mesh size and stress. The trends are nearly identical for each mesh size, with deviations occurring in the region of maximum stress (near the 2-mm boundary between the bone and muscle), as expected (Fig. 4). The percent change from the mean of the maximum stresses was calculated for each mesh size. The 0.2-mm element size produced ~2.5% change from the mean. For this study, we felt that further mesh refinement would increase computational time without improving the accuracy of the trends in

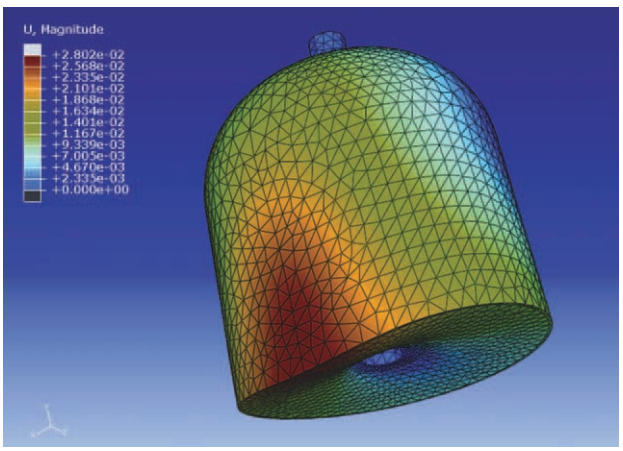

FIGURE 3. Final deformed state. [Color figure can be viewed in the online issue, which is available at wileyonlinelibrary.com.]

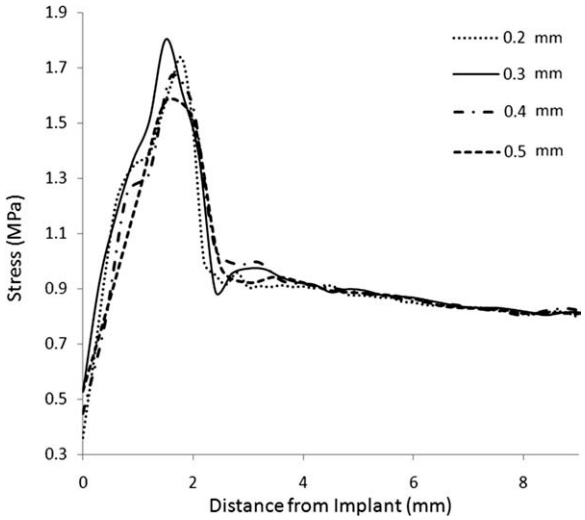

FIGURE 4. Mesh convergence data. The trends show all peak stresses located near the 2-mm boundary for each element size. The 2-mm bone case was used for each element size.

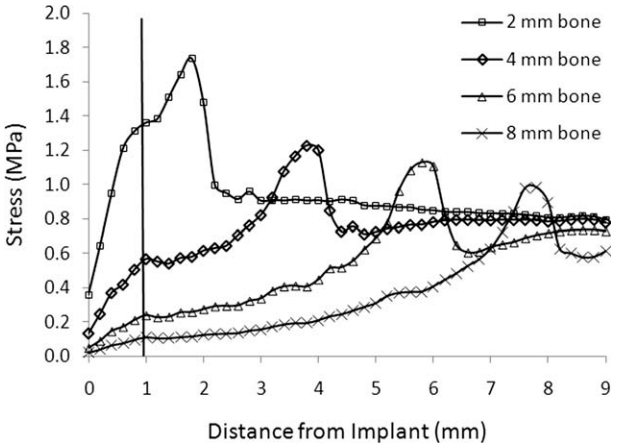

FIGURE 5. Stress distribution for each bone case at maximum loading. Vertical line at 1 mm indicates location of artificial stress riser due to geometric effects of curved edges near implant interface.

stress distribution as a function of bone thickness; thus the 0.2-mm element size was used for all simulations since it provided a robust enough mesh to accurately capture the stress concentrations in the regions of interest. Also, stresses were measured at a height of 0.5 mm from the skin–bone interface based on a mesh study that examined stress variation as a function of skin thickness. A height of 0.5 mm from the skin–bone interface was shown to produce maximum stresses and thus all measurements were taken at this location. In addition, stress contour plots at the posterior surface of the analysis region were created to qualitatively show the distribution of stresses around the implant for each bone case.

Four sets of bone cases were tested, with the 2-mm bone case serving as the baseline cortical bone thickness after implant insertion. Although cortical bone thickness is anisotropic in the femur, it was assumed to be a uniform thickness of 2 mm since an idealized model was used. The results indicate that stresses started low at the implant interface, and then sharply rose, peaking near the bone–muscle boundary at a distance of ~2 mm from the implant, then sharply decreasing and leveling off at 3 mm from the implant (Fig. 5). In addition, a small peak was observed near the 1-mm mark, as a result of an artificial stress riser (Fig. 5) due to the curved edges at the implant interface [Fig. 1(b)]. This geometry creates a 0.5-mm void space between the skin and the bone, which results in an increased deformation in the skin and the observed stress riser near the 1-mm mark. Stress distribution contours in the analysis region were symmetrical about the radial direction, with stresses concentrated circumferentially around the analysis region at a distance of ~2 mm from the implant [Fig. 6(a)].

The 4-mm bone case showed trends similar to the 2-mm bone case, with stresses gradually increasing at the implant interface before sharply rising and peaking near the bone–muscle boundary at 4 mm, then rapidly decreasing at 5 mm before leveling off (Fig. 5). Another artificial stress riser was observed near the 1-mm mark. In addition, stress contours indicated a shift of concentrated stresses from 2 to 4 mm along the radial direction from the implant [Fig. 6(b)]. The 6- and 8-mm bone cases showed the same trends as in the 2 and 4 mm cases, with peak stresses concentrated near bone–muscle boundary at distances of 6 and 8 mm, respectively, from the implant (Fig. 5). Stress contours also showed the progressive shift of concentrated stresses from distances of 6–8 mm, indicating a further dissipation of stresses away from the implant [Fig. 6(c,d)].

Stresses were further reduced at the skin-implant interface as bone thickness increased from 6 to 8 mm. Stress analysis at the skin-implant interface showed a rapid decrease in stress as bone thickness increased from 2 to 8 mm—stresses at the implant interface were reduced by more than ~62.7%, ~86.4%, and ~94.1% as bone thickness increased from 2 to 4, 6, and 8 mm, respectively. A linear relationship between stress and applied load was observed for each loading case (Fig. 7). In addition, the slope of the line was reduced by more than a factor of 2 for every 2 mm of added bone, indicating that data extrapolation could be performed to estimate stresses for higher applied loads at a given cortical bone thickness.

DISCUSSION

The FE results showed that adding a ring of bone around the abutment had a profound impact on reducing stresses near the skin-implant interface of OI prostheses. Stresses were concentrated in the analysis region along the underlying bone–muscle boundary, which progressively shifted radially from the implant as bone was added. Peak skin stresses observed near the bone–muscle boundary were due to the compliant characteristics of muscle tissue. Since the skin was tied to both the underlying bone and muscle tissues, stresses were concentrated in the muscle layer since its compliant properties caused higher deformations. Stresses in the skin proximal to the bone–soft tissue boundary had

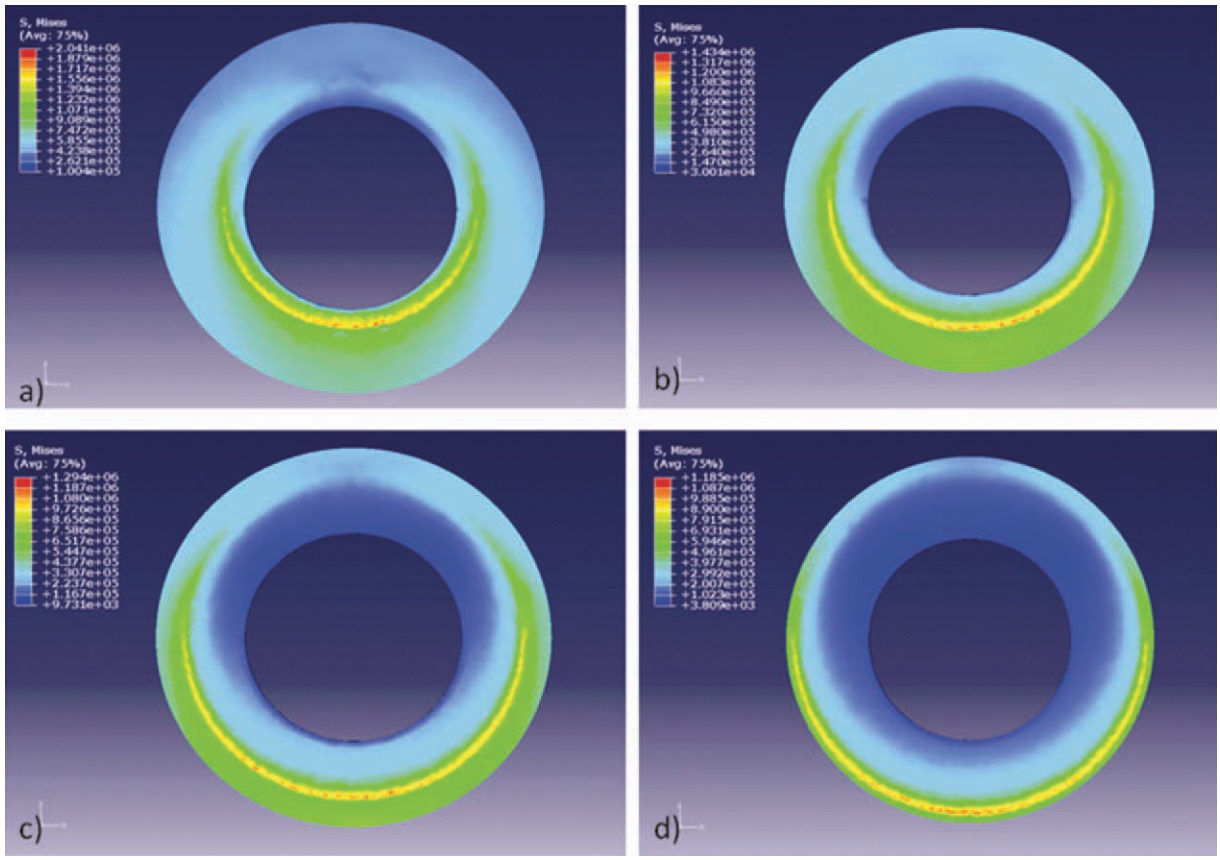

FIGURE 6. Stress contours at posterior surface of analysis region. Slices taken at a distance of 0.5 mm from skin–bone interface. (a–d) 2-, 4-, 6-, and 8-mm bone cases, respectively. [Color figure can be viewed in the online issue, which is available at wileyonlinelibrary.com.]

lower stress concentrations, as expected, due to the rigid bone material properties. Thus, the added bone served as a mechanical stabilizer, shifting concentrated stresses away from the implant interface, resulting in a drastic decrease in stresses at the implant interface. Addition of 2, 4, and 6 mm of base material to the baseline 2-mm case reduced stresses by more than 60%, 80%, and 90%, respectively, indicating an increased immobilization of soft tissue near the implant interface. Furthermore, increasing the diameter of base material around the abutment caused stress distributions to dissipate circumferentially, reducing localized stress concentrations [Fig. 6(b–d)], and creating a wider buffer zone around the percutaneous abutment. It is also important to note that this study presents the use of a natural material, bone tissue, for providing increased surface area for skin adhesion; other techniques utilizing artificial materials may also be used to stabilize the skin at the abutment interface.

The results from this study provide promising data that indicate that soft tissue immobilization near the exit site can improve outcomes of skin in-growth into porous titanium implants and may reduce infection rates.[18] The current biomaterials approaches attempt to create a permanent seal by promoting skin in-growth into the titanium implants.[2,4,9,11,12] However, shear stresses near the implant interface may break down this skin-implant seal. Data from this study suggest that adding rigid material under the skin around the abutment will help dissipate stresses away from the implant interface, assisting in stabilizing any new biocompatible skin-implant interface.

Research groups have employed several techniques, either through surgical procedures or implantation of subcutaneous devices, to increase the surface area for skin adhesion. Bone capping is one approach that could be used and can be accomplished in a variety of ways. Branemark et al.

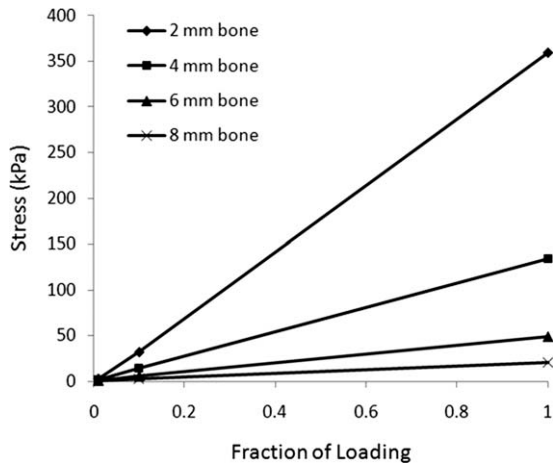

FIGURE 7. Linearity trends in applied loads.

have successful developed a bone capping technique for their osseointegration system. They preserve the cancellous bone remnants from drilling for the titanium implant, concentrate these bone fragments by centrifuge and then pack this bone paste over the implant, which is placed 1–2 cm beyond the end of the bone. After adequate healing time, a firm bone ring forms around the abutment to which the skin can then be adhered.[13] A bone plug with autogenous bone grafts, such as the iliac crest could also be used.[19] Bone would be grafted from the iliac crest to the distal portion of femur to widen the cortex. A periosteal bridge could also be formed around the distal portion of the femur to promote osteogenesis and widen the cortex. This technique is widely used in amputation osteoplasty in an effort close the medullary canal and form a bridge between the tibia and fibula to enhance loading bearing capabilities in transtibial amputees.[20]

Alternatively, a subcutaneous flange that stabilized the skin could also be used, as reported by Kang et al.[12] With this technique, a porous titanium flange is attached to the distal end of the implant. The flange is coated with hydroxyapatite to promote skin in-growth. Prior to suturing the skin to the flange, subcutaneous fat is removed from skin to ensure a direct contact between the flange and skin to optimize adhesion. A cap (Stanmore Implants Worldwide) and washer (Algeo, Liverpool, UK) are fastened to the outer distal skin around the percutaneous abutment to provide a firm contact with the flange to promote skin in-growth. The adhesion of skin to rigid biocompatible materials would have the same effect of buffering the shear forces as the bone capping techniques; a broad area for skin adhesion would minimize stresses at the abutment interface. In addition, it has been reported by Perry et al. that antimicrobial agents alone cannot prevent infections in percutaneous implants in sheep models, and the study concludes that creating a stable, immobile skin interface is essential to help prevent infections.[21] Data from this study can be used as a model for creating a skin immobilization system for percutaneous implants.

Although interesting results are presented in this study, a number of limitations exist. First, the FE model studied represents an idealized model since patient-specific geometries were not available. Thus, the symmetric stress distribution contours observed in this study would not be expected. Regardless, geometric asymmetries would not have a profound impact on stress distribution in the buffer region since we assume that the surface area for skin adhesion is increased uniformly around the bone. Thus, we would expect similar trends in stress reduction as a function of bone thickness in patient-specific geometries. Next, a simplified Neo–Hookean model for the skin was used since quasistatic loads were studied. However, it is well documented that skin behaves viscoelastically; thus, future studies that incorporate more complex, time-dependent skin models may be useful.[22,23] In addition, ambulatory loading conditions, such as walking, were not studied. This initial study did not consider many variables such as torsional loading, torsion shear, or cumulative stresses over time. However, the quasidynamic condition of sitting, as specified in this model, provides a relevant physiological setting in which to examine a large shear force and the effects of increased bone thickness on stress reduction, since these loading conditions could produce nearly constant and relatively high-shear forces on the skin.

For the purpose of this study, the simplified skin model provided useful data since the absolute stress values were not of importance; rather, the relative changes in stress concentration and distribution as cortical bone thickness increased were most relevant. However, it is important to note that our model assumed isotropic skin properties, though studies have shown that skin behaves in an anisotropic manner.[24,25] Thus, future studies should examine the effects of directionality on stress distribution, as this could have a significant impact on trends in stress reduction. In addition, this model did not account for slip conditions between the skin and muscle. For this initial study, this interaction was not considered in order to simplify the model. The degree of impact these conditions would have on stress distribution at the skin-implant interface is unknown; thus, future studies should incorporate slip conditions to gain better insight on how this boundary condition would change the trends of stress reduction as a function of cortical bone thickness. Finally, these models should be validated with experimental data. Unfortunately, data on skin adherence to cortical bone or a subcutaneous implant are not readily available.

The results from this modeling study provide clinically relevant insights for stress stabilization near the percutaneous abutment of OI prostheses. Specifically, a broadened base of support for skin adhesion at the distal end of the femur results in a drastic decrease in stress at the skin-abutment interface. Stress dissipation away from the percutaneous exit site not only protects the integrity of skin adhesion to the bone, but may also reduce infection rates by reducing the amount of soft tissue breakdown at the skin-implant interface and provide a better seal for the system.

REFERENCES

1. Hagberg K, Branemark R. One hundred patients treated with osseointegrated transfemoral amputation prostheses—Rehabilitation perspective. J Rehabil Res Dev 2009;46:331–344.
2. Pendegrass CJ, Goodship AE, Blunn GW. Development of a soft tissue seal around bone-anchored transcutaneous amputation prostheses. Biomaterials 2006;27:4183–4191.
3. Xu W, Crocombe AD, Hughes SC. Finite element analysis of bone stress and strain around a distal osseointegrated implant for prosthetic limb attachment. Proc Inst Mech Eng H 2000;214:595–602.
4. Pitkin M, Raykhtsaum G, Pilling J, Galibin OV, Protasov MV, Chihovskaya JV, Belyaeva IG, Blinova MI, Yudintseva NM, Potokin IL, Pinaev GP, Moxson V, Duz V. Porous composite prosthetic pylon for integration with skin and bone. J Rehabil Res Dev 2007;44:723–738.
5. Branemark R, Branemark PI, Rydevik B, Myers RR. Osseointegration in skeletal reconstruction and rehabilitation: A review. J Rehabil Res Dev 2001;38:175–181.
6. Lee WC, Doocey JM, Branemark R, Adam CJ, Evans JH, Pearcy MJ, Frossard LA. FE stress analysis of the interface between the bone and an osseointegrated implant for amputees—Implications to refine the rehabilitation program. Clin Biomech (Bristol, Avon) 2008;23:1243–1250.
7. Hagberg K, Branemark R, Gunterberg B, Rydevik B. Osseointegrated trans-femoral amputation prostheses: Prospective results

of general and condition-specific quality of life in 18 patients at 2-year follow-up. Prosthet Orthot Int 2008;32:29–41.
8. von Recum AF. Applications and failure modes of percutaneous devices: A review. J Biomed Mater Res 1984;18:323–336.
9. Pendegrass CJ, Gordon D, Middleton CA, Sun SN, Blunn GW. Sealing the skin barrier around transcutaneous implants: In vitro study of keratinocyte proliferation and adhesion in response to surface modifications of titanium alloy. J Bone Joint Surg Br 2008;90:114–121.
10. Knowles NG, Miyashita Y, Usui ML, Marshall AJ, Pirrone A, Hauch KD, Ratner BD, Underwood RA, Fleckman P, Olerud JE. A model for studying epithelial attachment and morphology at the interface between skin and percutaneous devices. J Biomed Mater Res A 2005;74:482–488.
11. Pendegrass CJ, Middleton CA, Gordon D, Jacob J, Blunn GW. Measuring the strength of dermal fibroblast attachment to functionalized titanium alloys in vitro. J Biomed Mater Res A 2010;92: 1028–1037.
12. Kang NV, Pendegrass C, Marks L, Blunn G. Osseocutaneous integration of an intraosseous transcutaneous amputation prosthesis implant used for reconstruction of a transhumeral amputee: Case report. J Hand Surg Am 2010;35:1130–1134.
13. Tillander J, Hagberg K, Hagberg L, Branemark R. Osseointegrated titanium implants for limb prostheses attachments: Infectious complications. Clin Orthop Relat Res 2010;468:2781–2788.
14. Xu W, Xu DH, Crocombe AD. Three-dimensional finite element stress and strain analysis of a transfemoral osseointegration implant. Proc Inst Mech Eng H 2006;220:661–670.
15. Teran J, Sifakis E, Blemker SS, Ng-Thow-Hing V, Lau C, Fedkiw R. Creating and simulating skeletal muscle from the visible human data set. IEEE Trans Vis Comput Graph 2005;11:317–328.
16. Tran HV, Charleux F, Rachik M, Ehrlacher A, Ho Ba Tho MC. In vivo characterization of the mechanical properties of human skin derived from MRI and indentation techniques. Comput Methods Biomech Biomed Eng 2007;10:401–407.
17. Xu W XD, Crocombe AD. Three-dimensional finite element stress and strain analysis of a transfemoral osseointegration implant. Proc Inst Mech Eng Part H 2006;220:661–670.
18. Chou TG, Petti CA, Szakacs J, Bloebaum RD. Evaluating antimicrobials and implant materials for infection prevention around transcutaneous osseointegrated implants in a rabbit model. J Biomed Mater Res A 2010;92:942–952.
19. Parsch D, Breitwieser T, Breusch SJ. Mechanical stability of structured bone grafts from the anterior iliac crest. Clin Biomech (Bristol, Avon) 2008;23:955–960.
20. DeCoster TA, Homedan S. Amputation osteoplasty. Iowa Orthop J 2006;26:54–59.
21. Perry EL, Beck JP, Williams DL, Bloebaum RD. Assessing periimplant tissue infection prevention in a percutaneous model. J Biomed Mater Res B: Appl Biomater 2010;92:397–408.
22. Silver FH, Freeman JW, DeVore D. Viscoelastic properties of human skin and processed dermis. Skin Res Technol 2001;7: 18–23.
23. Holt B, Tripathi A, Morgan J. Viscoelastic response of human skin to low magnitude physiologically relevant shear. J Biomech 2008; 41:2689–2695.
24. Reihsner R, Menzel EJ. On the orthogonal anisotropy of human skin as a function of anatomical region. Connect Tissue Res 1996; 34:145–160.
25. Nickell S, Hermann M, Essenpreis M, Farrell TJ, Kramer U, Patterson MS. Anisotropy of light propagation in human skin. Phys Med Biol 2000;45:2873–2886.